Spectroscopic investigation of elastic and magnetoelastic properties of CoFeB thin films

IOP Publishing Journal of Physics D: Applied Physics
J. Phys. D: Appl. Phys. 49 (2016) 145003 (6pp) doi:10.1088/0022-3727/49/14/145003

Spectroscopic investigation of elastic and magnetoelastic properties of CoFeB thin films

M Gueye[1], F Zighem[1], M Belmeguenai[1], M S Gabor[2], C Tiusan[2] and D Faurie[1]

[1] Laboratoire des Sciences des Procédés et des Matériaux, CNRS, Université Paris 13-Sorbonne Paris Cité, F-93430, Villetaneuse, France
[2] Center for Superconductivity, Spintronics and Surface Science, Technical University of Cluj-Napoca, Str. Memorandumului No. 28 RO-400114, Cluj-Napoca, Romania

E-mail: zighem@univ-paris13.fr and faurie@univ-paris13.fr

Received 25 June 2015, revised 19 January 2016
Accepted for publication 26 January 2016
Published 10 March 2016

Abstract

Magneto-stress coupling has been studied in $Co_{20}Fe_{60}B_{20}$ thin films of varying thicknesses (10, 20 and 250 nm) deposited onto flexible substrate. It has been investigated by measuring the magnetic resonance under uniaxial (tensile or compressive) applied stresses *in situ*. The benchmark state, in terms of elastic and magnetic properties, was studied by combining Brillouin light scattering experiments and magnetic resonance experiments on flat samples. The deduced parameters are thickness-independent and close to the ones obtained using rigid substrates. A large uniaxial anisotropy proportional to the applied uniaxial stress is found, which is well fitted by considering an isotropic saturation magnetostriction coefficient. Finally, the angular dependence of the resonance field with in-plane biaxial stresses is probed and explained using a simple analytical model.

Keywords: ferromagnetic resonance, magnetoelastic anisotropy, flexible systems

(Some figures may appear in colour only in the online journal)

1. Introduction

The recent development of magnetic devices, such as giant magnetoresistance, magnetic tunnel junctions or magnetoimpedance systems [1–8], fabricated on flexible substrates leads to the need to properly scrutinize the strain effect on the static and dynamic magnetic properties. Indeed, these devices are made by depositing a metallic medium (films or nanostructures) onto a flexible system for which a slight bending effort can lead to high in-plane uniaxial or biaxial stresses during their usage. Indeed, these stress and strain fields modify the static magnetization distribution inside nanostructures [9] and induce non-negligible planar magnetic anisotropies in thin films that are undesirable for some applications [10–12]. Furthermore, the integration of such materials in flexible devices, especially in the case of magnetic tunnel junctions [2, 3], requires very smooth interfaces between the different constituents.

For this purpose, amorphous alloys, such as $(Co_{1-x}Fe_x)_{1-y}B_y$, seem to be ideal candidates for flexible magnetic devices [13] since they can grow smoothly leading to well defined interfaces and have already proven themselves on rigid substrates [14–16]. CoFeB thin films have attracted much attention from researchers in spintronics, especially after the accessions of very high values of tunnel magnetoresistance (>200%). The main application lies in the development of basic tunnel junctions of this material. However, to expand the application scope of these CoFeB-based tunnel junctions, it is crucial to study other properties than simple magnetoresistance, such as the magnetostrictive effect, for uses such as sensors using flexible substrates. Indeed, a strain gauge is a sensor whose resistance varies with applied force; it converts force, pressure, tension and weight into a change in electrical resistance which can then be measured. Hence, the high magnetoresistance value of tunnel junctions made of CoFeB offers the

potential of developing strain gauges of high sensitivity [17, 18]. Thus, the joint use of magnetoelastic properties and magnetoresistance can be applied to connect electrical resistance and elastic strains. However, it is important to know the relationship between strains, stresses and magnetic anisotropy in these alloys. We therefore propose to jointly explore elastic and magnetoelastic properties of CoFeB thin films on flexible substrates, and especially look at the stress state effect on magnetic anisotropy since this plays an important role in tunnel junction properties. Until now, only the effect of uniaxial bending on magnetic anisotropy has been studied [13, 19], and exploration of the still unclear elastic properties, which should depend on alloy composition, is lacking.

In this paper, the influence of uniaxial and biaxial bending on the magnetic properties of CoFeB thin films deposited onto flexible substrate is carefully studied. In this respect, amorphous $Co_{20}Fe_{60}B_{20}$ (CFB hereafter) thin films of 10, 20 and 250 nm have been deposited onto a Kapton® substrate (125 μm thick) using a magnetron sputtering system. The CFB films were deposited at room temperature under an argon pressure of 1 m Torr and a rate of 0.1 nm.s^{-1}. The film was then capped with a 5 nm thick Ta layer. The amorphous behavior of all the films has been verified by x-ray diffraction measurements The elastic properties of the films were studied by measuring the velocity of surface acoustic waves (SAWs) using a Brillouin light scattering (BLS) system [20] while the magnetic and magnetoelastic properties were probed by measuring the magnetic resonance using a microstripline ferromagnetic resonance (MS-FMR) setup [21, 22].

2. Elastic properties by Brillouin scattering

A deep study of elastic coefficients has been achieved by Brillouin scattering to obtain the whole elastic properties. Here, because of the amorphous structure of the CFB films, the elastic properties can be considered as isotropic. Therefore, only two elastic coefficients (Poisson's ratio (ν_f) and Young's modulus (Y_f)) influence the SAW frequencies.

The Brillouin scattering technique is based on inelastic scattering of light. In the specific case of opaque thin films on substrates, one can only probe SAWs such as the Rayleigh wave and the Sezawa ones [23]. The Rayleigh wave is a slight material undulation confined at the top surface of the film. It has an elliptic polarization that lies in the sagittal plane defined by the propagation direction and the surface normal (xOz in figure 1). On the other hand, the Sezawa ones are standing waves in the film thickness. The Rayleigh velocity is mainly related to the shear elastic coefficient ($C_{44}^f = G_f$ for isotropic media [24]) while the harmonic Sezawa ones depends both on Y_f and G_f. Obviously, ν_f is directly related to these two last coefficients.

The light beam allows phonons to be probed that are thermally excited at room temperature. Because of the wave-vector conservation in the phonon–photon interaction, the wavelength of the revealed elastic waves is of the same order of magnitude as that of light. This means that the wavelength is much larger than the interatomic distances, so that the material can be described as a continuum within an effective-medium approach. A backscattering geometry has been adopted, see sketch in figure 1. A typical experimental spectrum of the 250 nm-CFB film is shown in blue; it should be noted that the elastic parameters (Y_f and ν_f) were extracted from the thicker film (250 nm) to avoid coupling effects (in an elastic point of view) with the polymer substrate. It was obtained with an incident angle $\xi = 65°$, so that the wave vector of the SAW is fixed to $k_{\parallel} = \frac{4\pi}{\Lambda}\sin\xi = 2.14 \times 10^5\,\mathrm{cm}^{-1}$, where $\Lambda = 5.32 \times 10^{-5}$ cm is the wavelength of the incident light (see figure 1). The Rayleigh and Sezawa (1st and 2nd harmonics) waves are clearly observed. The red line is a theoretical spectrum obtained by the simulation of the SAW frequencies and intensities of the thin film and by taking into account only the ripple mechanism for the scattered intensity. It has been calculated by using the formalism presented in [20]. Comparison between the experimental and the theoretical spectra leads to values of $Y_f = 160$ GPa ($\equiv 160 \times 10^{10}$ dyn.cm^{-2}), $G_f = 59$ GPa and $\nu_f = 0.37$. These values are consistent with those generally reported for metallic glasses, and follow the relationship between Young's modulus and shear modulus for this class of materials ($Y_f \simeq 2.6 G_f$) [25].

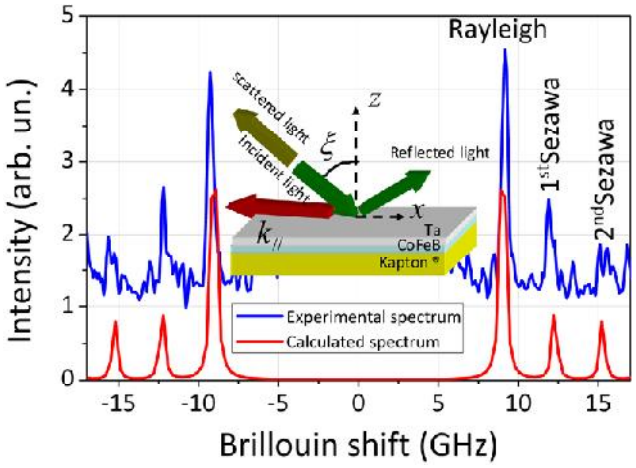

Figure 1. Experimental and theoretical Brillouin spectra of the 250 nm thick amorphous CoFeB thin layer deposited onto Kapton®. The blue (resp. red) line corresponds to the experimental (resp. theoretical) spectrum. Both Rayleigh and Sezawa peaks can be observed. The sketch illustrates the backscattering geometry used in the present experiment. The transferred wave-vector is fixed to $k_{\parallel} = 2.14 \times 10^5\,\mathrm{cm}^{-1}$.

3. Magnetomechanical coupling resulting from uniaxial bending

The magnetic and magnetoelastic properties of the films have been investigated through *in situ* (with respect to the applied stress) MS-FMR experiments. Indeed, uniaxial, tensile and compressive stresses have been applied to the films by gluing them on small pieces of aluminum blocks of circular cross-section of known radii R (1.32 cm, 3.22 cm, 4.16 cm, 5.92 cm, and infinite (flat surface)). Flexible but not stretchable elements can conform to any object with zero-Gaussian curvature, e.g. cylinder.

In the case of a metallic film (thickness d_f) deposited on a polymer substrate (thickness d_s), a high mechanical contrast (film Young's modulus Y_f (160 GPa) strongly different from the substrate one Y_s (∼4 GPa)) would lead to a change in neutral surface as compared to a bare substrate. Suo *et al* give the expression of the resulting longitudinal strain at the top surface ($\varepsilon_{xx}^{\text{top}}$) where the metallic film is confined [26]:

$$\varepsilon_{xx}^{\text{top}} = \pm\left(\frac{d_f + d_s}{2R}\right)\Gamma. \tag{1}$$

The sign of this strain depends on the sign of the curvature $\kappa = \pm\frac{1}{R}$ while Γ is defined as follows:

$$\Gamma = \frac{1 + 2\eta + \chi\eta^2}{(1+\eta)(1+\chi\eta)} \tag{2}$$

where $\eta = \frac{d_f}{d_s}$ and $\chi = \frac{Y_f}{Y_s}$. In this case, the expression of the uniaxial stress for the film ($\sigma_{xx}^{\text{applied}}$) is given by:

$$\sigma_{xx}^{\text{applied}} = Y_f \varepsilon_{xx}^{\text{top}}. \tag{3}$$

For very thin films (10 and 20 nm), Γ is higher than 0.99. Thus the expression (1) reduces to the so-called $\varepsilon_{xx} \simeq \pm\frac{d}{2R}$ with d the whole thickness that is roughly the substrate one [11]. For thicker films, the use of equation (1) is unavoidable; for example, $d_f = 250$ nm leads to $\Gamma \simeq 0.92$. Considering the Y_f value previously obtained by BLS, the different applied stresses for the thinner films (10 and 20 nm) are determined using equation (1): ±0.75 GPa, ±0.31 GPa, ±0.23 GPa, ±0.16 GPa and 0 GPa. The ones for the thicker thickness (i.e. 250 nm) are 8% lower than these last values. In these conditions, the maximum compressive and tensile strains are about 0.4%, which is relatively low. No surface instabilities or damages (wrinkles, cracks) have been observed by optical and atomic force microscopies. Tang *et al* [13] have reported the absence of cracks in amorphous $Co_{40}Fe_{40}B_{20}$ thin films for tensile strains lower than 1% and for a large range of thicknesses (10 to 200 nm).

Typical MS-FMR spectra recorded at different stress states are presented in figure 2. More details on the experimental setup can be found in [11]. All the spectra are vertically shifted by a value of ∼750 Oe (which corresponds to the resonance field of the non-strained spectrum). Moreover, the spectra recorded at +0.75 GPa and −0.75 GPa for the 20 nm film are vertically shifted for better presentation. These spectra were obtained with a magnetic field applied along the x axis (direction of the applied stress). Furthermore, the intensity reduction observed for the two spectra measured under non-zero stress (red and blue lines) as compared to the one measured at zero applied stress (black line) is essentially due to an obvious smaller probed magnetic volume by the microstripline. A positive (resp. negative) shift of the resonance field, defined as $\delta H_{\text{res}} = H_{\text{res}}(0) - H_{\text{res}}(\sigma_{xx})$, is observed when a tensile (resp. compressive) stress is applied to the film. These shifts are consistent with a positive magnetostrictive coefficient. Indeed, in the case of an isotropic material subjected to a uniaxial stress, the magnetoelastic energy can be written as:

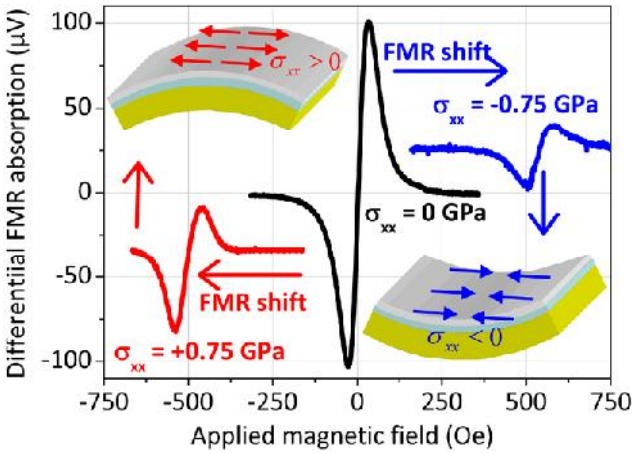

Figure 2. MS-FMR spectra measured for the 20 nm thin layer at different stress states with an applied magnetic field along the applied stress. Tensile stress (+0.75 GPa) leads to a positive shift while compressive stress (−0.75 GPa) leads to a negative one. The spectra have been vertically shifted for better comprehension.

$$E_{\text{me}} = -\frac{3}{2}\lambda\left(\gamma_x^2 - \frac{1}{3}\right)\sigma_{xx} \tag{4}$$

where λ is the isotropic magnetostriction coefficient and γ_x is the directional cosines of the magnetization $\vec{M}$. Thus, an effective magnetoelastic field, defined as $\vec{H}_{\text{me}} = -\vec{\nabla}_{\vec{M}} E_{\text{me}}$, can be introduced. For positive λ and σ_{xx}values, this field is aligned along the x direction, which leads to an easy axis that will decrease (positive shift) the resonance field of the uniform mode [21, 22], as experimentally observed. Moreover, one can note that the shifts presented in figure 2 are not symmetrical ($\delta H_{\text{res}} \simeq 500$ Oe for the positive shift and $\delta H_{\text{res}} \simeq -550$ Oe for the negative one). This asymmetry is due to the presence of an initial pre-stress state (before applied bending) of the whole sample which leads to an initial uniaxial anisotropy, which could be significant[10–13, 21, 22]. This pre-stress state is due to the large Young's modulus mismatch between the polymer substrate (4 GPa) and the CFB films (160 GPa), and it leads to a slight curvature along a given direction during the elaboration process [10].

The resonance field of the uniform mode can be analytically evaluated and compared to the experimental measurements by considering the total magnetic energy density of the films composed of the: Zeeman, dipolar and magnetoelastic energies (the exchange contribution is not considered for the uniform mode). With the assumption of a planar and uniform magnetization always parallel to the applied magnetic field, the expression of the uniform mode resonance field can be derived as the sum of two contributions: $H_{\text{res}} = H_1 + H_2$ with [22]:

$$H_1 = \left[\left(2\pi M_s + \frac{3\lambda\sigma_{xx}}{2M_s}\sin^2\varphi_H\right)^2 + \left(\frac{2\pi f}{\gamma}\right)^2\right]^{0.5} - 2\pi M_s \tag{5}$$

$$H_2 = \frac{-3\lambda\sigma_{xx}}{4M_s}(1 + 3\cos 2\varphi_H) \tag{6}$$

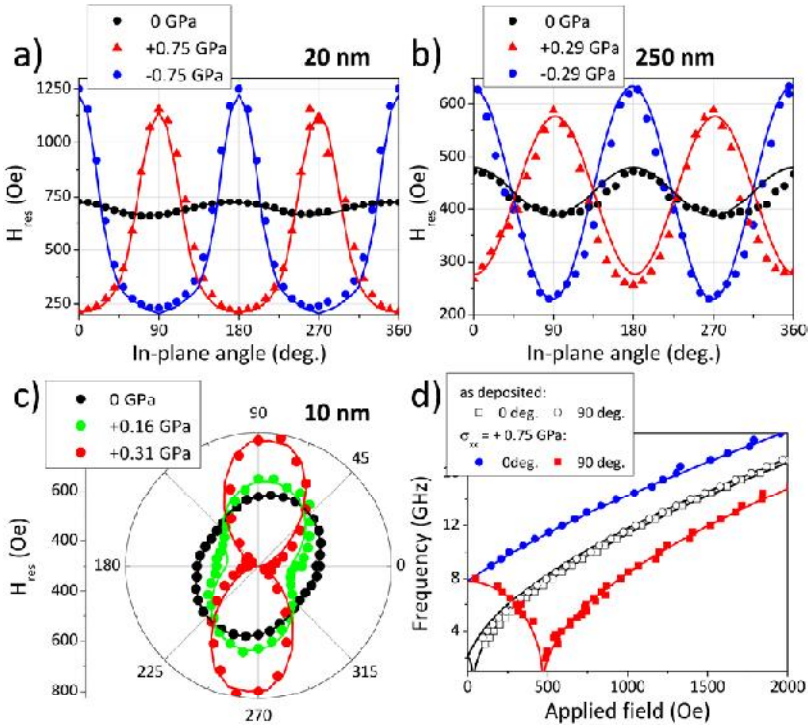

Figure 3. Angular dependencies of the uniform mode resonance field for the (a) 20 nm (with $f = 9.5$ GHz), (b) 250 nm (with $f = 8$ GHz) and (c) 10 nm (with $f = 8$ GHz) films. The frequency dependence of the uniform mode is presented in (d) for the 20 nm-thick film along the easy and hard axis (0 deg. and 90 deg.) when applying a tensile stress (blue and red symbols). In all graphs, the full lines are best fits to the experimental data by using equations presented in the text.

where f, γ, M_s and φ_H are respectively the microwave driven frequency, the gyromagnetic factor, the saturation magnetization and the angle in between the direction of the applied stress (x direction) and the applied magnetic field. Since the magnetic fields applied in the MS-FMR experiments are above saturation, only H_2 is stress-dependent (in first approximation) since H_1 essentially depends on $\frac{2\pi}{\gamma}$ and $2\pi M_s$, that are larger than $\frac{3\lambda}{2M_s}\sigma_{xx}$. Note that the initial uniaxial anisotropy due to the pre-stress state of the samples is taken into account by simply adding an *ad hoc* uniaxial anisotropy in the above expression [21].

The angular dependencies of the resonance field are presented in figure 3 where data at 0 GPa are obtained for the flat sample. One can see the presence of an initial uniaxial anisotropy in all cases, as previously discussed. The angular dependence of H_{res} (figures 3(a)–(c)) and the frequency variation of the uniform mode (figure 3(d)) at 0 GPa allowed the magnetization at saturation and the gyromagnetic factor of the films to be determined, which are found to be almost the same for the whole investigated thicknesses: $M_s = 1030$ emu.cm^{-3} (confirmed by magnetometry measurements) and $\gamma = 1.948 \times 10^7$ Hz.Oe^{-1}. The initial anisotropy is almost constant and is equal to around 40, 45 and 30 Oe for the 10 nm, 20 nm and 250 nm films, respectively. From these values, a mean residual stress of around 50 MPa is deduced for all the studied samples, which is in good agreement with values previously deduced for other materials [10, 11, 22].

Figure 3 also shows the angular dependence of H_{res} measured at different stress states by bending all the samples. Full symbols correspond to the experimental data while continuous lines show the best fits of the data using the equations previously presented where the only undetermined parameter is the saturation magnetostriction coefficient λ. Being given the M_s, Y and γ values determined from the flat sample measurements, a value of 23×10^{-6} is deduced. Note that the different fits presented in figure 3 are obtained by minimizing the total energy density which is more rigorous than simply using equations (5) and (6).

In figures 3(a) and (b), one can observe that the initial uniaxial anisotropy (pre-stress state) leads to non symmetrical angular dependencies for two opposite values of the applied stress for the 20 nm and 250 nm thick films. Indeed, the initial anisotropy field is aligned along y direction ($\varphi_H = 90°$) which means that the initial pre-stress is compressive along the x direction. Thus, the angular dependence is reinforced (resp. reduced) when the sample is compressively (resp. tensely) stressed along x. Interestingly, for the 10 nm thick film (figure 3(c)), the initial anisotropy is slightly titled with respect to the x axis and remains slightly titled for an applied stress of 0.16 GPa. All these behaviors are well explained by the analytical expression of the resonance field with the pre-determined values (Y , M_s, and γ). Figure 3(d) shows the frequency variation of the uniform mode measured at 0 GPa and at +0.75 GPa for an applied magnetic field along x and y directions ($\varphi_H = 0°$ and 90°). A uniaxial anisotropy due to the magnetomechanical coupling is clearly seen and well described by the model. It is interesting to note that the experimental effective anisotropy field (H_u, sum of the initial anisotropy field and the one due to the applied stress) measured from the data recorded along

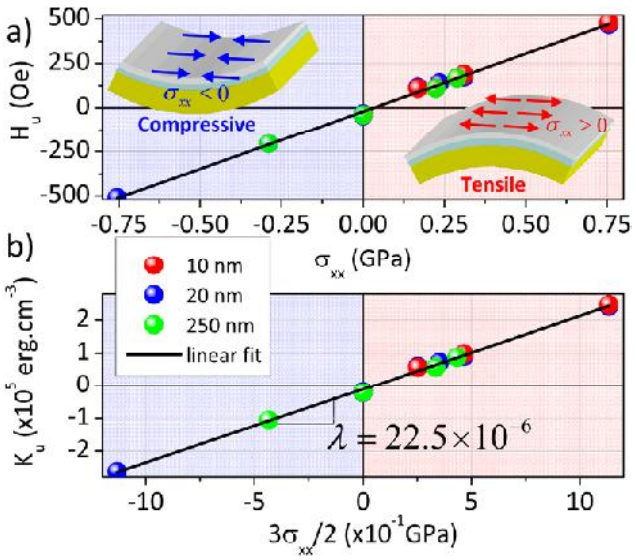

Figure 4. (a) Effective anisotropy field H_u variation as a function of the applied stress. (b) Variation of the effective anisotropy constant (K_u), deduced from equation (7), as a function of the ratio $\frac{3}{2}\sigma_{xx}$; the linear fit slope directly gives the magnetostriction coefficient $\lambda = 22.5 \times 10^{-6}$.

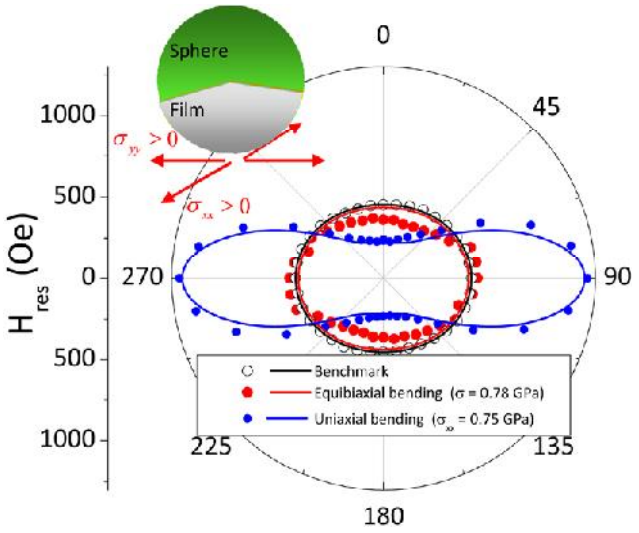

Figure 5. Angular dependence of the resonance field for the 20 nm thick film. Symbols are experimental data while full lines are calculated thanks to the analytical models. Black open circles are data from the benchmark state while the red ones correspond to the experimental equibiaxial state (with $\sigma \simeq 0.78$ GPa). The blue circles are measurements coming from uniaxial bending with a uniaxial stress ($\sigma_{xx} \simeq 0.75$ GPa) comparable to the equibiaxial σ.

the y ($\varphi_H = 90°$) axis ($H_u \simeq 480$ Oe obtained from the experimental softening of the frequency, see figure 3(d)) is in good agreement with the one resulting from the angular dependence of H_{res} ($H_u \simeq 475$ Oe from figure 3(a) by using this formula: $2H_u \simeq H_{res}(\varphi_H = 90) - H_{res}(\varphi_H = 0)$).

Figure 4(a) reports the measured effective anisotropy field H_u as a function of the applied strains. The extreme values are roughly $\pm$500 Oe and aligned in a single straight line which reinforces the thickness-independent observed magnetomechanical behavior of the studied thin films. In addition, the saturation magnetostriction coefficient may be also determined by using the following relation [12]:

$$K_u \simeq \frac{3}{2}\lambda\sigma_{xx} \tag{7}$$

where K_u is the anisotropy constant of the effective anisotropy field H_u: $H_u = \frac{2K_u}{M_s}$. This direct determination of λ is illustrated in figure 4(b) where the slope of the linear fit directly gives the λ value ($\sim 22.5 \times 10^{-6}$) in excellent agreement with the one deduced from the whole MS-FMR experiments.

4. In-plane anisotropy smoothing due to biaxial bending

The magnetomechanical properties of these films were finally studied by performing compressive equibiaxial test. For this purpose, the 20 nm thick film was glued onto a 2 cm radius sphere (see schematic of figure 5). In the case of an equibiaxial bending [27], the biaxial stress can be expressed as a function of the sphere radius (R_{sphere}):

$$\sigma = \sigma_{xx}^{applied} = \sigma_{yy}^{applied} = \pm Y_f^*\left(\frac{d_f + d_s}{2R_{sphere}}\right)\Gamma \tag{8}$$

with $Y_f^* = \frac{Y_f}{1-\nu}$ the biaxial modulus. In these conditions, an in-plane equibiaxial stress of around $\sigma \simeq +0.78$ GPa is expected for the 20 nm film (close to the uniaxial stress value generated by the cylinder whose radius is 1.32 cm); the expression of the resonance field becomes:

$$H_{res} = \left[\left(2\pi M_s + \frac{3\lambda\sigma}{2M_s}\right)^2 + \left(\frac{2\pi f}{\gamma}\right)^2\right]^{\frac{1}{2}} - 2\pi M_s - \frac{3\lambda\sigma}{2M_s}. \tag{9}$$

Obviously, the equibiaxial stress induced by gluing the film on the sphere leads to a vanishing φ_H dependence and a slight shift of the H_{res} baseline lower or higher than the unstressed state depending on the sign of the equibiaxial stress and of the magnetostriction coefficient [28]. Thus, this equibiaxial stress acts as an out-of-plane anisotropy, defined for instance by K_{out}, which reduces or increases the value of the effective magnetization $4\pi M_{eff} = 4\pi M_s - \frac{2K_{out}}{M_s}$ [29]. Figure 5 depicts the experimental (black open circles) and calculated (black line) angular dependence of the 20 nm thick film in the benchmark state. The experimental angular dependence of the equibiaxial stress state is represented by the full red circles. As expected, this angular dependence shows that the obtained anisotropy is very far from the uniaxial case previously obtained for a similar stress value of around +0.75 GPa (with $R = 1.32$ cm) shown by the blue symbols and line on figure 5. However, a weak planar uniaxial anisotropy (~50 Oe), superimposed to the initial one, is observed. Indeed, the red line shows the calculated ideal equibiaxial angular dependence of H_{res}. The small deviations of these experimental results from the theory are most probably due to small imperfections during equibiaxial bending. Indeed, using a flexible but non-stretchable polymer foil, such as Kapton®, it is impossible to conform

perfectly on an object showing a non-zero Gaussian curvature (defined as the product of the principal curvatures) [30].

5. Conclusion

The magnetomechanical properties of $Co_{20}Fe_{60}B_{20}$ have been investigated. Brillouin light scattering experiments allow the determination of the elastic parameters (Young's modulus and Poisson's ratio) that are not easily attainable by other techniques (partly due to the amorphous character of the films). The magnetic and magnetoelastic behavior of the films were thus studied by probing the magnetic resonance of the uniform mode. The magnetization at saturation and the gyromagnetic factor are thickness independent (in the studied range of thicknesses) and are very close to the one obtained in CFB films deposited onto more conventional substrates (rigid ones). The influence of uniaxial (compressive and tensile) applied stress in the resonance field of the uniform mode was studied and well explained by the combination of the presented standard model and the pre-determined elastic parameters. Finally, in-plane equibiaxial stresses which in theory only translated the resonance field of a few hundreds of Oe (depending on the amplitude of these stresses) were applied to the film. A small planar uniaxial anisotropy is observed and is attributed to a deviation from the perfect equibiaxial test.

Acknowledgments

The authors would like to thank Noël Girodon-Boulandet, engineer-assistant at LSPM-CNRS, for the design and the mechanical fabrication of the table and the arm supporting the MS-FMR experiment motorization. MSG acknowledges the financial support of UEFISCDI through PN-II-RU-TE-2014-4-1820—SPINCOD research grant, number 255/01.10.2015. CT acknowledges the Exploratory Research Project, SPINTAIL PN-II-ID-PCE-2012-4-0315, No. 23/29.08.2013, and POS CCE ID. 574, code SMIS-CSNR 12467, for financial support.

References

[1] Lin G, Makarov D, Melzer M, Si W, Yan C and Schmidt O G 2014 *Lab Chip* **14** 4050
[2] Barraud C, Deranlot C, Seneor P, Mattana R, Dlubak B, Fusil S, Bouzehouane K, Deneuve D, Petroff F and Fert A 2010 *Appl. Phys. Lett.* **96** 072502
[3] Bedoya-Pinto A, Donolato M, Gobbi M, Hueso L E and Vavassori P 2014 *Appl. Phys. Lett.* **104** 062412
[4] Melzer M, Kaltenbrunner M, Makarov D, Karnaushenko D, Karnaushenko D, Sekitani T, Someya T and Schmidt O G 2015 *Nat. Commun.* **6** 6080
[5] Fernández E, Kurlyandskaya G V, García-Arribas A and Svalov A V 2012 *Nanoscale Res. Lett.* **7** 230
[6] Agra K, Mori T J A, Dorneles L S, Escobar V M, Silva U C, Chesman C, Bohn F and Corrêa M A 2014 *J. Magn. Magn. Mater.* **355** 136
[7] Li B, Kavaldzhiev M N and Kosel J 2015 *J. Magn. Magn. Mater.* **378** 499
[8] Alfadhel A, Li B, Zaher A, Yassine O and Kosel J 2014 *Lab Chip* **14** 4362
[9] Streubel R, Thurmer D J, Makarov D, Kronast F, Kosub T, Kravchuk V, Sheka D D, Gaididei Y, Schäfer R and Schmidt O G 2012 *Nano Lett.* **12** 3961
[10] Gueye M, Zighem F, Faurie D, Belmeguenai M and Mercone S 2014 *Appl. Phys. Lett.* **105** 052411
[11] Gueye M, Wague B M, Zighem F, Belmeguenai M, Gabor M S, Petrisor T, Tiusan C, Mercone S and Faurie D 2014 *Appl. Phys. Lett.* **105** 062409
[12] Yu Y *et al* 2015 *Appl. Phys. Lett.* **106** 162405
[13] Tang Z *et al* 2014 *Appl. Phys. Lett.* **105** 103504
[14] Ikeda S, Miura K, Yamamoto H, Mizunuma K, Gan H D, Endo M, Kanai S, Hayakawa J, Matsukura F and Ohno H 2010 *Nat. Mater.* **9** 721
[15] Kanai S, Yamanouchi M, Ikeda S, Nakatani Y, Matsukura F and Ohno H 2012 *Appl. Phys. Lett.* **101** 122403
[16] Djayaprawira D D, Tsunekawa K, Nagai M, Maehara H, Yamagata S, Watanabe N, Yuasa S, Suzuki Y and Ando K 2005 *Appl. Phys. Lett.* **86** 092502
[17] Tavassolizadeh A, Meier T, Rott K, Reiss G, Quandt E, Hölscher H and Meyners D 2013 *Appl. Phys. Lett.* **102** 153104
[18] Tavassolizadeh A, Hayes P, Rott K, Reiss G, Quandt E, Meyners D 2015 *J. Magn. Magn. Mater.* **384** 308
[19] Zhang H, Li Y Y, Yang M-Y, Zhang Bao B, Yang G, Wang S-G, Wang K-Y 2015 *Chin. Phys.* B **24** 077501
[20] Rossignol C, Perrin B, Bonello B, Djemia P, Moch P and Hurdequint H 2004 *Phys. Rev.* B **70** 094102
[21] Zighem F, Faurie D, Mercone S, Belmeguenai M and Haddadi H 2013 *J. Appl. Phys.* **114** 073902
[22] Zighem F, El Bahoui A, Moulin J, Faurie D, Belmeguenai M, Mercone S and Haddadi H 2014 *J. Appl. Phys.* **116** 123903
[23] Fillon A, Jaouen C, Michel A, Abadias G, Tromas C, Belliard L, Perrin B and Djemia Ph 2013 *Phys. Rev.* B **88** 174104
[24] Pham T, Faurie D, Djemia P, Belliard L, Le Bourhis E, Goudeau P, Paumier F 2013 *Appl. Phys. Lett.* **103** 041601
[25] Wang W H 2012 *Prog. Mater. Sci.* **57** 487
[26] Suo Z, Ma E Y, Gleskova H and Wagner S 1999 *Appl. Phys. Lett.* **74** 1177
[27] Timoshenko S and Woinowsky-Krieger S 1959 *Theory of Plates and Shells* (Singapore: McGraw-Hill)
[28] Zighem F, Belmeguenai M, Faurie D, Haddadi H and Moulin J 2014 *Rev. Sci. Instrum.* **85** 103905
[29] Zighem F, Roussigné Y, Chérif S M and Moch P 2008 *J. Phys.: Condens. Matter* **20** 125201
[30] Rogers J A, Someya T and Huang Y 2010 *Science* **327** 1603